improved by the periparticular molecules, which stands beside the QD as electron donors and transfer the electric condition using their molecular polarity.

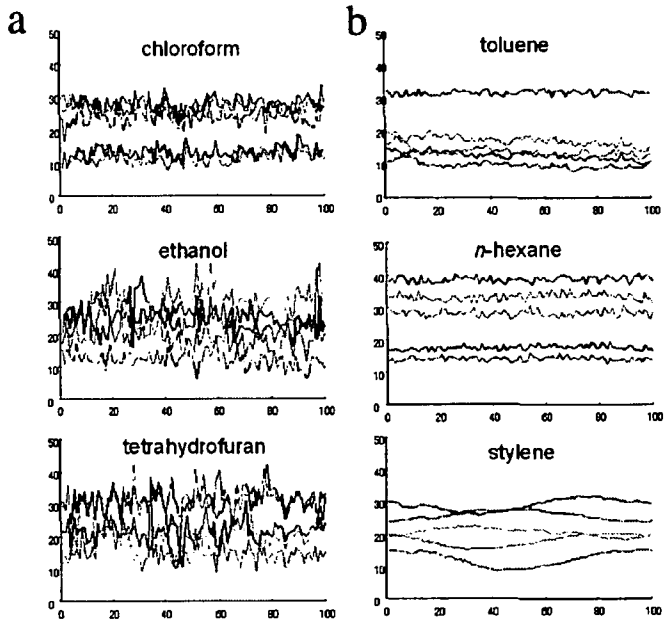

Fig. 4. Polarity of the solvent regulates the frequency of the millisecond oscillation. The millisecond oscillation of QD-COOH in (a) polar organic solvents; chloroform, ethanol, and tetrahydrofuran, and (b) non-polar inorganic solvents; toluene, n-hexane, and styrene, were observed on the evanescent field by the total-reflective fluorescent microscopy with a CCD camera unit FASTCAM®. The blinking frequency of each monodispersed QD (n=6) on each one millisecond is measured by one millisecond exposure. QDs. *x*-axis indicates the time [millisecond] and *y*-axis indicates the fluorescence intensity. Data shown are one of three independent experiments that gave the same results.

4 CONCLUSIONS

We propose a novel photophysical property on the fluorescent intensity of QD called millisecond oscilation. Millisecond oscillation has direct relationship with the increase/decrease of fluorescence intensity of QD-solution. The previous reports mentioned that not only core materials but the surface covered molecules which surround QD regulate the photoluminescent intensity of QD. In addition, we stated in this article that external environmental molecules which stand beside the QDs also affect the fluorescent intensity via millisecond oscillation. These results suggested that the surface and environmental molecules surrounded QDs act as the way to transfer the excited electron on QDs. Our study provided the criteria to determine the suitable molecules that covered QDs without losing higher fluorescence activity.

Acknowledgments

We thank Dr. Koichi Tanaka and his colleagues (Kobe Natural Compounds Co.Ltd, Kobe, Japan) for their efforts about synthesizing colloidal quantum dots. FASTCAMR MAXI-I^2 CCD camera unit was kindly provided by Photoron corp., (Tokyo, Japan). This work was

supported mainly by a Medical Techniques Promotion Research Grant H14-nano-004 from the Ministry of Health, Labor and Welfare of Japan (K. Yamamoto), and supported partly by a research fellowship grant from the Japan Society of Promotion of Science (A. Hoshino).

References

[1] F. Koberling, A. Mews, and T. Basche, "Oxygen-induced blinking of single CdSe nanocrystals," *Adv. Mater.* **132,** 672-676 (2001) [doi: 10.1002/1521-4095(200105)13:9<672::AID-ADMA672>3.0.CO;2-W].

[2] S. Hohng and T. Ha, "Near-complete suppression of quantum dot blinking in ambient conditions," *J. Am. Chem. Soc.* **126,** 1324-1325 (2001) [doi: 10.1021/ja039686w].

[3] K. T. Shimizu, W. K. Woo, B. R. Fisher, H. J. Eisler, and M. G. Bawendi, "Surface-enhanced emission from single semiconductor nanocrystals," *Phys. Rev. Lett.* **89,** 117401 (2002) [doi: 10.1103/PhysRevLett.89.117401].

[4] J. K. Jaiswal, H. Mattoussi, J. M Mauro, and S. M. Simon, "Long-term multiple color imaging of live cells using quantum dot bioconjugates," *Nat. Biotechnol.* **21,** 47-51 (2003) [doi: 10.1038/nbt767]

[5] K. Hanaki, A. Momo, T. Oku, T. Komoto, S. Maenosono, Y. Yamaguchi, and K.Yamamoto, "Semiconductor quantum dot/albumin complex is a long-life and highly photostable endosome marker," *Biochem. Biophys. Res. Commun.* **302,** 496-501 (2003) [doi:10.1016/S0006-291X(03)00211-0].

[6] M. Dahan, S. Levi, C. Luccardini, P. Rostaing, B. Riveau, and A. Triller, "Diffusion dynamics of glycine receptors revealed by single-quantum dot tracking," *Science* **302,** 442-445 (2003) [doi: 10.1126/science.1088525].

[7] A. Hoshino, K. Hanaki, K. Suzuki, and K. Yamamoto, "Applications of T-lymphoma labeled with fluorescent quantum dots to cell tracing markers in mouse body," *Biochem. Biophys. Res. Commun.* **314,** 46-53 (2004) [doi: 10.1016/j.bbrc.2003.11.185].

[8] E. R. Goldman, A. R. Clapp, G. P. Anderson, H. T. Uyeda, J. M. Mauro, I. L. Medintz, and H. Mattoussi, "Multiplexed toxin analysis using four colors of quantum dot fluororeagents," *Anal Chem.* **76,** 684-688 (2004) [doi: 10.1021/ac035083r].

[9] A. Hoshino, K. Fujioka, M. Suga, Y. F. Sasaki, T. Ohta, M. Yasuhara, K. Suzuki, and K. Yamamoto, "Quantum dots targeted to the assigned organelle in living cells," *Microbiol. Immunol.* **48,** 985-994 (2004).

[10] A. Hoshino, K. Fujioka, N. Manabe, S Yamaya, Y. Goto, M. Yasuhara, and K. Yamamoto, "Simultaneous multicolor detection system of the single-molecular microbial antigen with total internal reflection fluorescence microscopy," *Microbiol. Immunol.* **49,** 461-470 (2005).

[11] E. B. Voura, J. K. Jaiswal, H. Mattoussi, and S. M. Simon, "Tracking metastatic tumor cell extravasation with quantum dot nanocrystals and fluorescence emission-scanning microscopy," *Nat. Med.* **10,** 993-998 (2004) [doi:10.1038/nm1096].

[12] X. Gao, Y. Cui, and R. M. Levenson, and L. W. Chung, and S. Nie, "*In vivo* cancer targeting and imaging with semiconductor quantum dots," *Nat. Biotechnol.* **22,** 969-976 (2004) [doi: 10.1038/nbt994].

[13] R. G. Neuhauser, K. T. Shimizu, W. K. Woo, S. A. Empedocles, M. G. Bawendy, "Correlation between fluorescence intermittency and spectral diffusion in single semiconductor quantum dots," *Phys. Rev. Lett.* **85,** 3301-3304. (2000) [doi:10.1103/PhysRevLett.85.3301].

[14] N. Eiha, S. Maenosono, K. Hanaki, K. Yamamoto, and Y. Yamaguchi, "Collective fluorescence oscillation in a water dispersion of colloidal quantum dots," *Jpn. J. Appl. Phys.* **42,** 310-313 (2003) [doi: 10.1143/JJAP.42.L310].

[15] T. Uematsu, J. Kimura, and Y. Yamaguchi, "The reversible photoluminescence enhancement of a CdSe/ZnS nanocrystal thin film," *Nanotech.* **15,** 822-827 (2004) [doi:10.1088/0957-4484/15/7/019].

[16] J. Kimura, T Uematsu, S. Maenosono, and Y. Yamaguchi, "Photoinduced fluorescence enhancement in CdSe/ZnS quantum dot submonolayers sandwiched between insulating layers: influence of dot proximity," *J. Phys. Chem. B* 108, 13258-13264 (2004) [doi: 10.1021/jp048406b].

[17] X. Peng, J. Wickham, and A. P. Alivisatos, "Kinetics of II-VI and III-V colloidal semiconductor nanocrystal growth: focusing of size distributions," *J. Am. Chem. Soc.* **120;** 5343.(1998) [doi:10.1021/ja9805425].

[18] E. R. Goldman, G. P. Anderson, P. T. Tran, H. Mattoussi, P. T. Charles, and J. M. Mauro, "Conjugation of luminescent quantum dots with antibodies using an engineered adaptor protein to provide new reagents for fluoroimmunoassays," *Anal Chem.* **74,** 841-847 (2002) [doi: 10.1021/ac010662m].

[19] T. Uematsu, S. Maenosono, and Y. Yamaguchi, "Photoinduced fluorescence enhancement in mono- and multilayer films of CdSe/ZnS quantum dots: dependence on intensity and wavelength of excitation light," *J. Phys. Chem. B* **109,** 8613-8618 (2005) [doi: 10.1021/jp050328k].

[20] A. Hoshino, K. Fujioka, T. Oku, M. Suga, Y. F. Sasaki, T. Ohta, M. Yasuhara, K. Suzuki, and K. Yamamoto, "Physicochemical properties and cellular toxicity of nanocrystal quantum dots depend on their surface modification," *Nano. Lett.* **4,** 2163-2169 (2004) [doi: 10.1021/nl048715d].

[21] J. Tang and R. A. Marcus, "Mechanisms of fluorescence blinking in semiconductor nanocrystal quantum dots," *J. Chem. Phys.* **123,** 054704 (2005) [doi: 10.1063/1.1993567].

[22] J. Yao, D. R Larson, H. D. Vishwasrao, W. R. Zipfel, and W. W. Webb, "Blinking and nonradiant dark fraction of water-soluble quantum dots in aqueous solution," *Proc. Natl. Acad. Sci. USA.* **102,** 14284-14289 (2005) [doi: 10.1073/pnas.0506523102].

[23] J. Tang and R. A. Marcus, "Diffusion-controlled electron transfer processes and power-law statistics of fluorescence intermittency of nanoparticles," *Phys. Rev. Lett.* **95,** 107401 (2005) [doi: 10.1103/PhysRevLett.95.107401].

[24] R. Hardman, "A toxicologic review of quantum dots: toxicity depends on physicochemical and environmental factors," *Environ. Health Perspect.* **114,** 165-72 (2006) [doi: 10.1289/ehp.8284].

[25] S. Jeong, M. Achermann, J. Nanda, S. Ivanov, V. I. Klimov, and J. A. Hollingsworth, "Effect of Thiol-Thiolate equilibrium on the photophysical properties of aqueous CdSe/ZnS nanocrystal quantum dots," *J. Am. Chem. Soc.* **127,** 10126-10127 (2005) [doi: 10.1021/ja042591p].

Kenji Yamamoto (M.D., Ph.D.) is the director of International Clinical Research Center at Research Institute, International Medical Center of Japan. He graduated from the University of Tokyo school of medicine in 1985 and received his Ph.D. degree in Medical Science (bacteriology) from the University of Tokyo in 1989. He is the author of more than 100 journal papers of bacteriology and theoretical biology. His current research interests include nanoparticles, biophotonics, chemical system engineering and nanobiomedical clinical research.

J Artif Organs (2007) 10:149–157
DOI 10.1007/s10047-007-0379-y

REVIEW

Akiyoshi Hoshino, Ph.D · Noriyoshi Manabe
Kouki Fujioka, Ph.D · Kazuo Suzuki, Ph.D
Masato Yasuhara, Ph.D · Kenji Yamamoto, MD, Ph.D

Use of fluorescent quantum dot bioconjugates for cellular imaging of immune cells, cell organelle labeling, and nanomedicine: surface modification regulates biological function, including cytotoxicity

Abstract With the development of nanotechnology, nanoscale products that are smaller than several hundred nanometers have been applied to all areas of science and technology. Nanoscale products, including carbon nanotubes, fullerene derivatives, and nanocrystal quantum dots (QDs), are wide spread as novel tools in various fields, not only in materials engineering, electronics, plastics, and the automobile and aerospace industries, but also in molecular biology and medicine. At present, QDs have been widely used in biological and medical studies because of their superior photoemission and photostability. Although the physical and chemical properties of QDs have been circumstantially investigated, little is known about any harmful effects of QDs on human health. Here we report on the toxicity and biological behavior of QDs in vitro and in vivo. The toxicity of the core constituent chemicals such as cadmium and selenium has been identified. Recently, the surface molecules surrounding QDs have been intensively investigated. Accumulating evidence that toxic surface-covering molecules showed their cytotoxicity and biomolecules conjugated with QDs maintained their biological effects indicates that at least the biological properties of QDs are attributable to the QD-capping material rather than to the core metalloid complex itself.

Key words Bioimaging · Cell trafficking · Cytotoxicity · Fluorescent probes · Nanocrystal

Received: August 28, 2006 / Accepted: January 31, 2007

A. Hoshino · N. Manabe · K. Fujioka · K. Yamamoto (✉)
International Clinical Research Center, Research Institute, International Medical Center of Japan, 1-21-1 Toyama, Shinjuku-ku, Tokyo 162-8655, Japan
Tel. +81-3-3202-7181; Fax +81-3-3202-7364
e-mail: backen@ri.imcj.go.jp

A. Hoshino · M. Yasuhara · K. Yamamoto
Department of Pharmacokinetics and Pharmacodynamics, Hospital Pharmacy, Tokyo Medical and Dental University Graduate School of Medicine, Tokyo, Japan

A. Hoshino · K. Suzuki
Department of Bioactive Molecules, National Institute of Infectious Diseases, Tokyo, Japan

Surface molecules define the properties of quantum dots

The fact that enormous advances in the field of nanotechnology could give conventional materials additional functionality based on nanoscale effects was predicted by Professor Ryogo Kubo in the 1960s,[1–3] but it has taken more than 40 years to realize the production of nanomaterials.[4,5] Nanomaterials that have specific functions based on nanometer size effects are now attracting much attention due to the intrinsic characteristics of nanomaterials, which are enhanced by their significantly larger surface area.[5–7] Currently, colloidal nanocrystal quantum dots (QDs) emitting very bright fluorescence are widely used in biological and in medical studies. These QDs are attractive fluorophores for multicolor imaging due to their broad absorption and narrow emission spectra, and are brighter and far more photostable than organic fluorescent dyes.[5–14]

Great quantities of artificial nanomaterials, including QDs, are produced and consumed on the unfounded assumption that nanomaterials are biologically and environmentally harmless: in fact, only a few studies have reported on the toxicity of such nanomaterials.[15–29] Recently, nanomaterial researchers have started to address nanomaterial-induced toxicity problems.[30–42] Why has research on the toxicity of nanomaterials progressed so slowly? The reason is attributed to some of the following factors: (1) Some research on nanomaterials has been performed under the premise that they are not toxic. Such research does not consider the viewpoint of toxicity. (2) Various kinds of nanomaterials that have their own unique properties have been synthesized, and a variety of QD concentrations has been reported. This makes it difficult to generally discuss the toxicity of QDs in terms of dose-dependent effects. (3) Sufficient quantities of nanomaterials cannot be supplied to carry out a series of toxicity studies. Some studies have been designed for toxicologists.

We and other nanomaterial researchers have reported that the behavior of QDs in the body [in terms of absorption, distribution, metabolism, and excretion (ADME)],

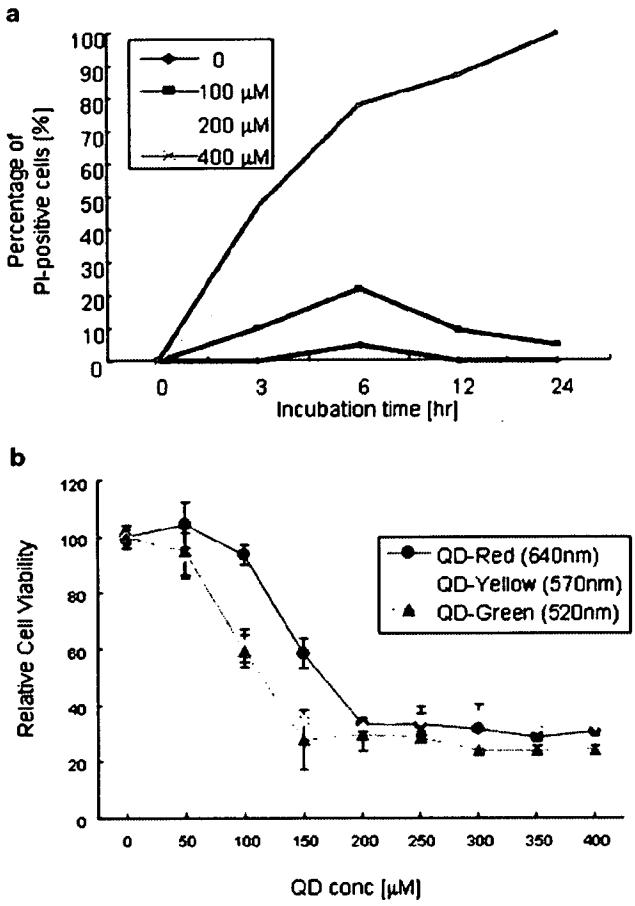

Fig. 1a,b. Dose- and particle-size-dependent quantum dot (*QD*) toxicity at high concentrations. **a** The cytotoxicity of QD520 (green) solution depends on its concentration. Vero cells were plated at 1×10^5 cells and stimulated with culture media alone or with QD520 at concentrations of 100, 200, and 400 μM. The cells were incubated for 3, 6, 12, and 24 h at 37°C. The cells were then harvested, stained for observation of dead cells with propodium iodide (*PI*), and measured by flow cytometric analysis. Fluorescence was measured by FACS Calibur (Beckton Dickinson). **b** Relative cell viabilities on exposure to different sized QDs were measured by MTT assay. Vero cells were plated at 1×10^5 cells on a 24-well plate and incubated for 12 h with the indicated concentration of QDs. The results show the averages of three separate experiments

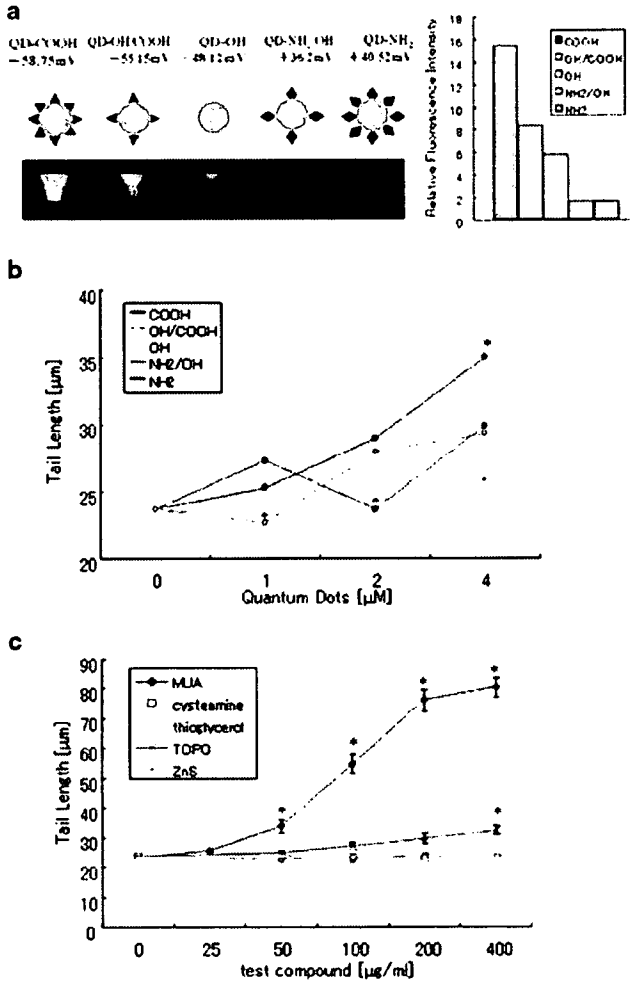

Fig. 2a–c. Surface-capping molecules participate in QD-induced cell damage and lethal cytotoxicy due to the toxicity of the molecules. **a** ZnS-coated CdSe nanocrystal QDs (fluorescence wavelength: approximately 518 nm, emitting green) were capped with 11-mercaptoundecanioc acid (*QD-COOH*), 2-aminoethanethiol (*QD-NH*$_2$), and 3-mercapto 1,2-propanediol (*QD-OH*) by thiol exchange reactons. Cartoon images and solution photos of QDs capped with the various surface molecules are shown on the *left*. The images of aqueous QD solutions (final concentration, 100 nM) were captured using a digital camera with 1/30 s exposure excited by 365-nm wavelength ultraviolet light (UV-A). The relative fluorescence intensity of each QD (shown on the *right*) was measured using fluorescence spectrometry. **b,c** The DNA-damaging effects of hydrophilic nanocrystalline QDs were assessed by comet assay. When WTK-1 cells were incubated with each sample, the fragmented DNA of apoptotic cells (called a comet tail) was eliminated from the nuclei by electrophoresis. The length of the comet tail stained with ethidium bromide was measured. **b** QD solutions induced genotoxic cell death. Cells were treated with QD-COOH (red), QD-NH2 (blue), QD-OH (yellow), QD-OH/COOH (orange), or QD-NH2/OH (green) for 2 h. **c** Chemicals capping QDs also induce cell death. Cells were treated with *MUA* (red), cysteamine (green), thioglycerol (yellow), *TOPO* (blue), or ZnS (orange) for 2 h. The difference between the means in the treated and control plates was compared with the Dunnett test after one-way ANOVA. $*P < 0.05$. Results are from three separate experiments

and their toxicity is dependent on multiple factors derived from both the individual physicochemical properties and the environmental conditions.[19,43–46] The toxicity of nanomaterials is primarily caused by their inherent physicochemical properties. In addition, some environmental factors, including oxidative, photolytic, and mechanical stability, often degrade QDs, resulting in additional toxicity.

A QD material has its own physicochemical properties that influence the toxicity dependent on the QD size, electric charge, concentration, and surface-coating materials, including capping materials and functional groups. We assessed the dose and size dependency of QD-mediated cytotoxicity at concentrations approximately 1000-fold those usually found in cellular applications. We observed the dose-dependent (Fig. 1a) and the size-dependent (Fig. 1b) cytotoxity of QDs.[42] The observed cytotoxicity is proportional to the number of QDs that are incorporated into the cells. In fact, we demonstrated that red QDs are incorporated into cells less easily than green ones.[42] Other groups have also demonstrated that QD-induced cell death was

due to chromatin condensation and that the size of QDs contributed to their subcellular distribution.[47] Moreover, cadmium and selenium, two of the most widely used constituent metals in the QD core crystal, are reported to cause acute and chronic toxicities in vertebrates when the QDs were irradiated to induce UV-mediated oxidative stress.[48] Furthermore, the capping materials and biomolecules that cover the QD surface also have a role in defining the total biological behaviour of the whole nanocrystal QD, including toxicity. We demonstrated that some surface-covering toxic molecules caused severe cytotoxicity in a dose-dependent manner, whereas some surface-covering less toxic molecules caused less cytotoxicity (Fig. 2). These results suggest that the bioactive behavior of QDs in biological systems is not only dependent on the nanocrystal particle itself but also on the biochemical properties of any surface-covering molecules.[43] These results provide evidence that some hydrophilic compounds that cap the surface of QDs are responsible for the biological effects of the whole QD complex. This result prompted us to attach drug molecules to QDs and observe whether the complex exerted its medicinal effect in vivo. First, we conjugated QDs with an antihypertension medicine, captopril.[49,50] Then we measured the effect of QD-conjugated captopril (QD-cap) in vitro; further, QD-cap was administered to spontaneously hypertensive rats to assess the effect of QD-medicine in vivo.[51] As expected, we were able to synthesize functional nanocomposit particles of QD and captopril without losing fluorescence activity or antihypertensive effects (Fig. 3). These results suggested that the surface treatment of nanocrystals (surface-capping with functional groups or with biomolecules covering the surface of QDs) can define the biological behavior of whole-nanocrystal QD complexes.[16,17,52–54]

Here, we consider that the toxicity of QDs in biological systems is not only dependent on the nanocrystal "core-particle" itself but also on the surface molecules. We observed no cytotoxicity from the ingredients of the QD core itself, suggesting that surface processing can overcome the toxicity of nanomaterials, unless the core structure itself is broken. Surface modification with functional molecules combined with nanomaterials can produce novel bionanomachines conforming to the functions designated by their surface molecules.[43,51] On the other hand, these results suggest that inappropriate treatment and disposal of QDs may still entail the risk of environmental pollution, including human health concerns, under certain conditions.

Quantum dots targeted to specific organelles in living cells

The result that the surface of a QD defines the total biological behavior prompted us to investigate the biological role of QDs with bioactive coverings; QDs conjugated with bioactive materials and signal peptides can be transported to the assigned organelle in living cells.[43] Some oligopeptides have been demonstrated to penetrate the cellular membrane by means of their protein transduction domains and

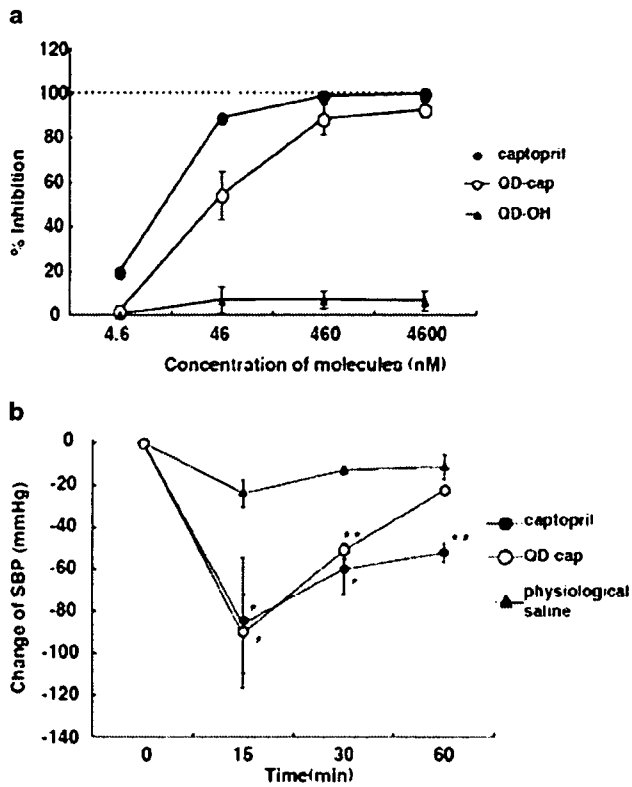

Fig. 3a,b. Captopril-capped QD (QD-cap) exerts its medicinal effect both in vitro and in vivo. Captoprol, an antihypertension medicine, was directly conjugated with QDs (QD-cap). Each QD-cap particle contains approximately 180 captopril molecules by peptide content assay. **a** The inhibition activity of angiotensin-1 converting enzyme (ACE, the target molecule of captopril) by QD-cap was measured by the Cushman and Cheung method. The data presented are the mean ± SD of triplicated samples. QD-cap shows inhibitory activity as well as capotpril alone. **b** QD-cap decreases the blood pressure in hypertensive rats. QD-cap (5 mg/kg) was injected i.v. into the SHR-SP spontaneous hypertensive rat via the carotid artery. After injection, the systolic blood pressure was measured by the tail-cuff method at the indicated times ($n = 3$). *SBP*, systolic blood pressure

to specificially locate their designated organelle. Previous studies have shown that protein transduction by nuclear localizing signal (NLS) peptides is an efficient method for delivering proteins into the nuclei of cells. In this study, we used two functional transport oligopeptides that localize to the nucleus or to mitochondria, and evaluated whether the QD–peptide complexes worked as specific functional supermolecules based on the original peptides. We designed a supermolecule comprising luminescent QDs conjugated with $R_{11}KC$[55] NLS peptides (QD-NLS), and with cytochrome-*c* oxidase VIII[56] mitochondria-targeting signal peptides (QD-MTS) (Fig. 4).

To trace the route of $R_{11}KC$ (NLS peptide) from the outer membrane to the nucleus in living cells, QD-NLS was added to cultured cells. Relocation from the cell membrane to nuclei was observed about 30s after incubation, and movement into the nucleolus was observed after 1 min. QD-NLS gradually accumulated throughout the whole nucleus during 15 min of incubation (Fig. 5a). Finally, we could visualize the motion of the QD-NLS being delivered

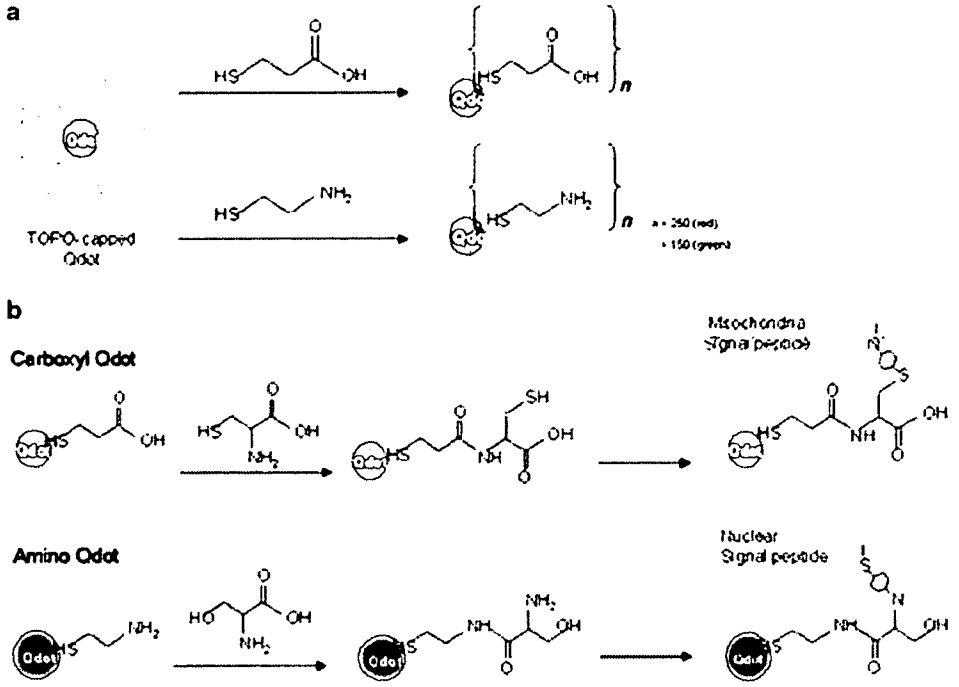

Fig. 4a,b. Schematic representation of peptide-conjugated QDs for specific organelle targeting and subcellular traffic imaging. **a** The QDs for peptide conjugation are based on carboxyl QDs (for anionic and hydrophilic peptides) or amino QDs (for highly cationic peptides). Chemically synthesized TOPO-capped QDs were replaced by mercaptopropanoic acid or cysteamine using thiol-exchange reactions. After the reaction, QDs were capped with approximately 250 carboxyl or amine groups per QD particle. **b** A two-step conjugation strategy for QD-oligopeptide probes. MPA-QD (*upper lane*, for anionic peptides) or cysteamine-QD (lower lane, for cationic peptides) was primarily coupled with the amine groups of cysteine or serine, respectively, by using EDC coupling reagents. Then amino acid-coated QDs were secondarily conjugated with these target peptides by coupling between their *N*-hydroxysuccinimidyl and maleimide groups

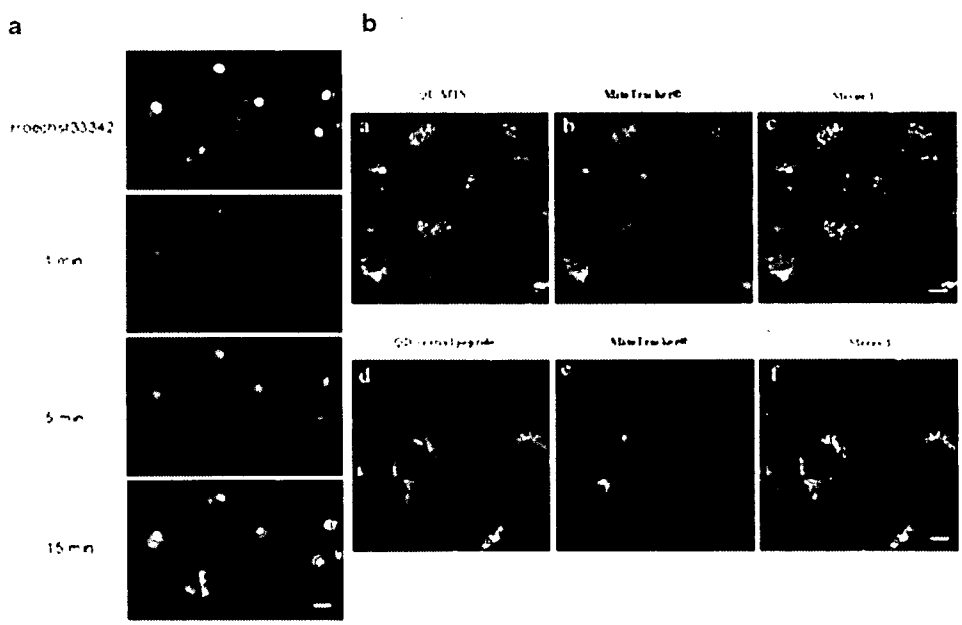

Fig. 5a,b. Visualizing the subcellular trafficking of organelle-localizing peptides using QDs. **a** Subcellular trafficking of QD-NLS for nuclei. Vero cells were prestained with Hoechst33342 (blue) and stimulated with QD640-R_{11}KC NLS peptides (emitting red, 1 μM final) for the indicated time at 37°C under a 5% CO_2 atmosphere with a culture fluorescence microscope (IM-310 system, Olympus, Tokyo, Japan). QD-NLS (red) was rapidly localized to nuclei after a few minutes' incubation. *Bars*, 10 μm. **b** Subcellular trafficking of QD-MTS for the mitchondrial membrane. Vero cells were cultured with QD520-Mito8 MTS peptide (emitting green, 1 μM) (*a–c*) or QD520-START negative control peptide (*d–f*) for 12 h at 37°C. Then cells were coincubated with MitoTracker (Molecular Probes, Engener OR) mitochondria staining reagents for an additional 1 h to confirm the mitochondrial localization. The cells were observed using confocal microscopy. The images were taken using a cooled CCD-camera equipped with confocal microscopy. (Bio-Rad, Hercules, CA). The fluorescence of QD-MTS (green) became merged with that of organic mitochondrial dyes, whereas the fluorescence of QD-control peptides did not. *Bars*, 20 μm, magnifications: ×80

into the nuclear compartment of cells using QD fluorescence. In addition, when cells were cultured with QD-MTS, the QD fluorescence became merged with the signal of mitochondrial fluorescent dye (Fig. 5b), whereas control QD-peptides did not. It is impossible for conventional fluorescent organic dyes to trace such a series of motions because of their labile fluorescent lifetime. Using this technique, we could trace the movement of tiny bioactive molecules (i.e., antibodies, cytokines, and medicinal chemicals) by QD fluorescence. Our techniques open up the possibility that QDs can reveal the transduction of proteins and peptides into specific subcellular compartments and could constitute a powerful tool for studying intracellular analysis in vitro and even in vivo.

We demonstrated that fluorescent QDs are a useful tool for tracing the motion of specific peptides as they selectively target specific organelles in living cells. In addition, these signal peptide–QD complexes have the ability to translocate across the cell plasma membrane and can subsequently home in on their specific targets, including the nucleus or the mitochondrial membrane.

The production of nanometer-sized materials with biological function is very important since we currently have no "designed material" that can arbitrarily penetrate nanometer-sized gaps such as those in the skin, membranes, and blood vessels, for example. This study demonstrates that the surface modification of nanoaparticles with functional molecules may function as bionanomachines conforming to the functions designated by their surface molecules. We have shown in this article that QDs with targeted peptides can be transported to nuclei and mitochondria. These techniques open up the possibility that QDs can reveal the transduction of proteins and peptides to specific subcellular compartments in vitro and even in vivo as a powerful tool for conducting intracellular analysis. Nanomaterials have the capacity to change even the concept of existing diagnosis and medical treatment by providing functions such as pharmacological and magnetic effects and by giving information of the specificity to tissue or organs in vivo.

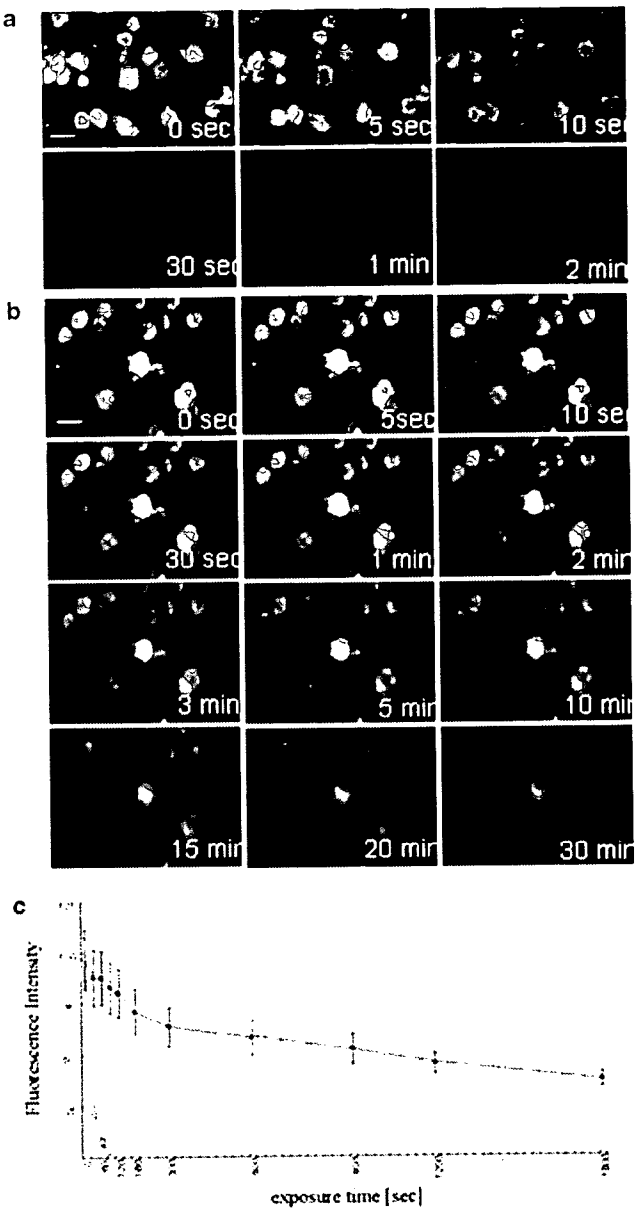

Fig. 6a–c. Comparison of photostability of QDs with that of conventional organic probes. Fluorescence photostability comparison of **a** QD-stained and **b** CFSE organic dye-stained $CD4^+$ T lymphocytes with continuous excitation from a 488-nm laser lamp. All images were taken using a D1X digital camera equipped with fluorescence microscope IX-81 at the indicated times using a 1.0-s exposure. **c** Comparison of the relative fluorescence intensity between QDs and the organic probe CFSE. *Open circles* indicate organic probes and *closed circles* are the QDs

QDs as cell-labeling dyes for immune cells

Here, we demonstrate the imaging of the movements of mouse lymphocytes and macrophages using QDs. First, we added a solution of QDs directly to lymphocytes, but failed to stain the cells. Aqueous QDs were easily aggregated in acidic or saline solutions, even if we produced aqueous modification. In addition, living cells do not incorporate substances that have a high electric charge, even if their metaphor sizes are small (i.e., sodium ions use a special ion channel to transport across the membrane). We have improved the methods for stabilizing QDs in biological solutions such as cell-culture media.[14,43] We examined several kinds of serum and intracellular protein to assess efficient stabilization. Among them, serum albumin with QDs was found to be suitable for labeling living cells. In this study, we assessed whether QDs could be applied to various applications using labeled cells for the purpose of long-duration tracing of living cells in vitro and in vivo. To take full advantage of the characteristics of QDs, we established the labeling of immune cells using QDs.[43]

Immune cells have specific features in that they move inside the body to act in host defense. Once pathogenic microbes attack the host, the immune cells are recruited

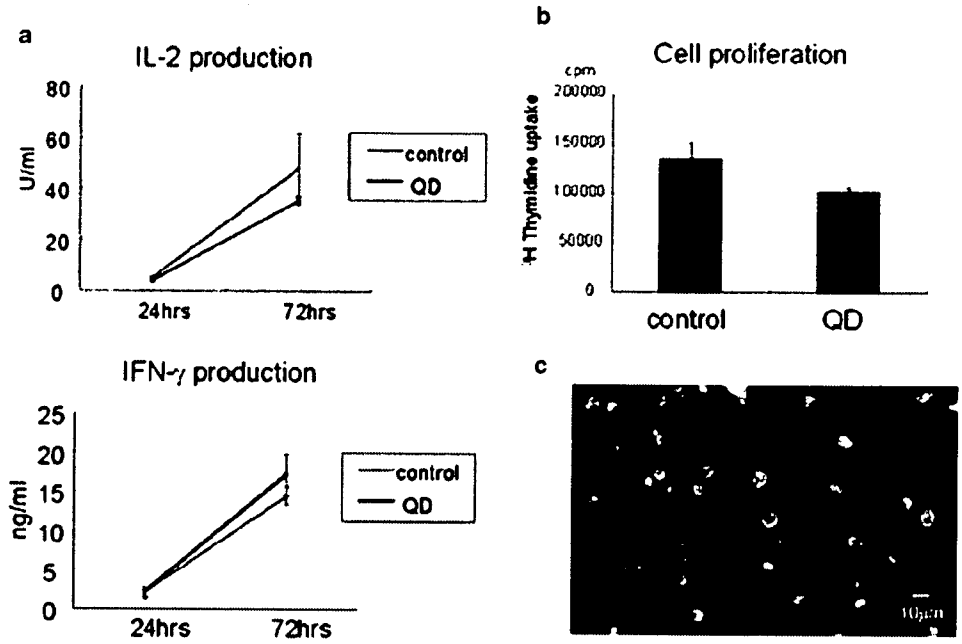

Fig. 7a–c. QDs have less effect on CD4⁺ T-lymphocyte function. Splenic CD4⁺ cells were collected from splenocytes of C57BL/6 mice and were positively selected by a MACS column using a mouse CD4⁺ T isolation kit. **a,b** Splenic CD4⁺ cells (5×10^5 cells/well in a 24-well plate) were prestained with or without 4 nM QD for 60 min and incubated without anti-CD3 stimulation for 4 h. Next, T lymphocytes (2.5×10^6 cells/well) were stimulated with anti-CD3 antibody (BD Pharmingen) and incubated for 12 h. Supernatant was collected after 24 h and 48 h and the cytokine IL-2 and IFN-gamma production was measured by ELISA. **c** T lymphocytes (2×10^6 cells/well) were stimulated with anti-CD3 antibody and then ^{3}H-thymidine (0.5 mCi) was added. After 16 h of stimulation, ^{3}H-thymidine uptake was measured. **d** Splenic CD4⁺ T lymphocytes were cultured for 5 days after being labeled with 4 nM QD and albumin solution for 60 min

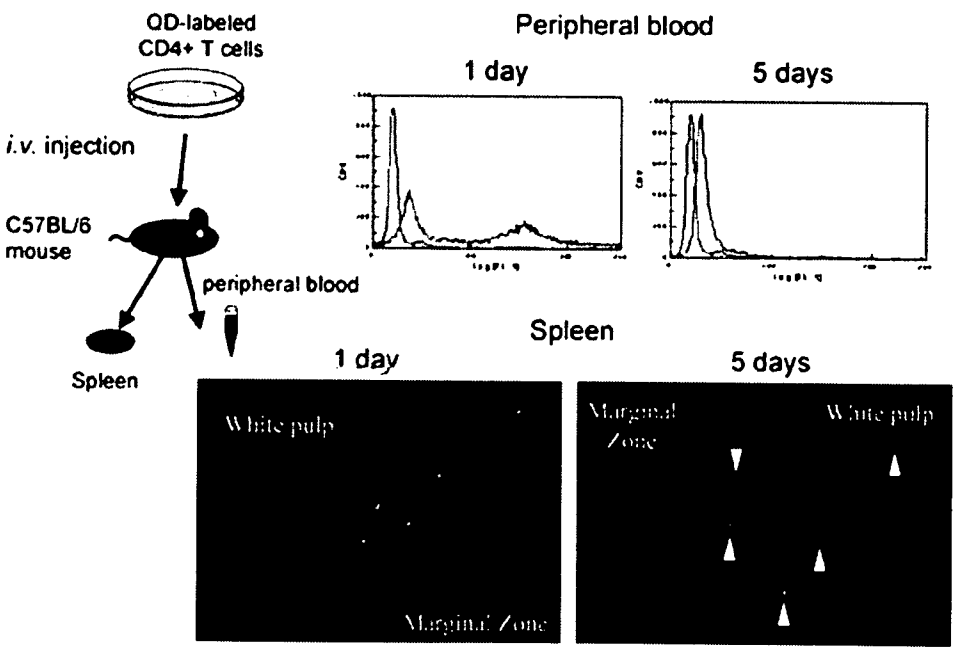

Fig. 8. Observation of QD-labeled CD4⁺ T lymphocytes in the peripheral blood and spleen. Mouse splenic CD4⁺ T lymphocytes were collected with a MACS column with a CD4⁺ T lymphocyte isolation kit. The collected lymphocytes were stained with 4 nM QD and albumin solution for 60 min. The stained CD4⁺ cells were intravenously injected into mice (1×10^6 cells/head). The mice were killed as indicated at day 1 and day 5. The peripheral blood leukocytes were harvested, separated by percoll gradient, and stained with propidium iodide to exclude dead cells from detection. The QD-positive lymphoctes were observed using FACS Calibur flow cytometry. QD-labeled cells could be detected in the blood circulation 5 days after injection. The fluorescence images of paraffin-embedded spleen sections at day 1 and day 5 were measured with fluorescence microscopy. *Arrowheads* indicate the location of QD-containing cells. Magnification ×200

from the circulation to the inflamed site and undertake specific actions. T lymphocytes play critical roles in the antigen-specific immune response. They continuously moved through the body, but activated T cells migrate to the inflamed site from blood vessels and promote bacterial killing by macrophages. T cells then leave the inflamed site and reenter the circulation. Therefore, it is very important to visualize the trafficking of T cells.

The labeling procedure of lymphocytes with QDs is quite simple. We purified CD4-positive T lymphocytes from murine splenocytes using magnetic beads (MACS system), and added QDs with albumin. Albumin-coated QDs were incorporated into the cells immediately after addition, and fluorescence was detected in the cytoplasm within 15 min; QDs were located in the endosomes. The cell labeling efficiency was quite high and almost all the cells were labeled. The fluorescent intensity increased, depending on the incubation time with QDs. Next we compared the photostability of QDs and an organic dye, Carboxyfluorescein Succinimidyl Ester (CFSE). CFSE faded completely within 1 min after exposure to an argon laser. Sometimes the fluorescence of CFSE disappeared during the focusing of the camera, resulting in missed photographs. In contrast, QD fluorescence was detected for over 30 min (Fig. 6). Thus, labeling with QDs is a strong tool especially for microscopic studies. Next, we examined whether QDs affect cell function. We labeled T lymphocytes with QDs and examined T-cell proliferation using tritiated-thymidine uptake and the production of cytokines, i.e., interleukin-2 (IL-2) and interferon-gamma (IFN-γ) productivity after activation of T cells with anti-CD3 antibody. It was found that there was no significant effect on cell function (Fig. 7). We found that when stimulated T cells were kept cultured for 5 days, QD-labeled living cells were still observed. These results indicate that QD-labeling is stable and does not affect either cellular activation or immune cell function. These data prompted us to trace QD-labeled cells in vivo. QD-labeled T cells were adoptive transferred to mice by injecting intravenously. QD-labeled cells were eliminated from the blood circulation promptly and became distributed throughout the whole body, but mostly in the spleen. One day later, cells were detected in the marginal zone of the spleen, and 5 days later, they were detected in the white pulp. Thus, QDs enabled visualization of target cells by time-lapse analysis (Fig. 8).

To summarize, visualization of the movements of immune cells was possible using the bright fluorescence of QDs. Labeling with QDs overcame the various problems described below in the detection of cells using fluorescent dyes.

1. Cells were easily labeled with QDs.
2. Fluorescence from QDs was far brighter and more stable, having clear advantages over conventional fluorescent dyes for cell labeling.
3. There was no significant effect on cell function after labeling of T cells with QDs.
4. QD-labeling enabled us to detect the distribution of the various cell types infiltrating various normal and inflamed tissues.

Conclusions

We conclude that the surface treatment of nanocrystals (surface covering functional groups and biomolecules capping the surface of QDs) determines the biological behavior of entire nanocrystal QD complexes. Advances involving the surface modification of QDs have enabled many novel biological experiments. We and other groups previously reported that QDs have been applied to some biological experiments, including long-term multicolor cell imaging in live cells,[7,43,57,58] and even in cancer immunotherapy with QDs.[13,59-64] This study suggests that QDs are excellent imaging agents for visualizing invisible vitreous in clinical situations. In addition, we are now concentrating our efforts on developing nanocrystals made from silicon, which are expected to show less inherent cytotoxicity.[65] We anticipate that these new imaging agents and methods will be used broadly, allowing disease to be diagnosed and understood easily and fully in the usual clinical setting and promoting safe and complete treatment for many medical situations.

References

1. Kubo R. Statistical-mechanical theory of irreversible processes. J Phys Soc Jpn 1957;12:570–586
2. Kubo R. Generalized cumulant expansion method. J Phys Soc Jpn 1962;17:1100–1120
3. Kubo R. Stochastic Liouville equations. J Math Phys 1962;4: 174–183
4. Springholz G, Holy VV, Pinczolits M, Bauer G. Self-organized growth of three-dimensional quantum-dot crystals with fcc-like stacking and a tunable lattice constant. Science 1998;282:734–737
5. Chan WC, Maxwell DJ, Gao X, Bailey RE, Han M, Nie S. Luminescent quantum dots for multiplexed biological detection and imaging. Curr Opin Biotechnol 2002;13:40–46
6. Chan WC, Nie S. Quantum dot bioconjugates for ultrasensitive nonisotopic detection. Science 1998;281:2016–2018
7. Jaiswal JK, Mattoussi H, Mauro JM, Simon SM. Long-term multiple-color imaging of live cells using quantum dot bioconjugates. Nat Biotechnol 2003;21:47–51
8. Hoshino A, Hanaki K, Suzuki K, Yamamoto K. Applications of T-lymphoma labeled with fluorescent quantum dots to cell tracing markers in the mouse body. Biochem Biophys Res Commun 2004;314:46–53
9. Gao X, Nie S. Quantum dot-encoded beads. Methods Mol Biol 2005;303:61–71
10. Xu H, Sha MY, Wong EY, Uphoff J, Xu Y, Treadway JA, Truong A, O'Brien E, Asquith S, Stubbins M, Spurr NK, Lai EH, Mahoney W. Multiplexed SNP genotyping using the Qbead system: a quantum dot-encoded microsphere-based assay. Nucleic Acids Res 2003;31: e43
11. Mandal SK, Lequeux N, Rotenberg B, Tramier M, Fattaccioli J, Bibette J, Dubertret B. Encapsulation of magnetic and fluorescent nanoparticles in emulsion droplets. Langmuir 2005;21:4175–4179
12. Bruchez M Jr, Moronne M, Gin P, Weiss S, Alivisatos AP. Semiconductor nanocrystals as fluorescent biological labels. Science 1998;281:2013–2016
13. Akerman ME, Chan WC, Laakkonen P, Bhatia SN, Ruoslahti E. Nanocrystal targeting in vivo. Proc Natl Acad Sci USA 2002;99: 12617–12621
14. Hanaki K, Momo A, Oku T, Komoto A, Maenosono S, Yamaguchi Y, Yamamoto K. Semiconductor quantum dot/albumin complex is a long-life and highly photostable endosome marker. Biochem Biophys Res Commun 2003;302:496–501
15. Borm PJ, Robbins D, Haubold S, Kuhlbusch T, Fissan H, Donaldson K, Schins R, Stone V, Kreyling W, Lademann J, Krutmann J, Warheit

D, Oberdorster E. The potential risks of nanomaterials: a review carried out for ECETOC. Part Fibre Toxicol 2006;3:11
16. Bottero JY, Rose J, Wiesner MR. Nanotechnologies: tools for sustainability in a new wave of water treatment processes. Integr Environ Assess Manag 2006;2:391–395
17. Garnett MC, Kallinteri P. Nanomedicines and nanotoxicology: some physiological principles. Occup Med (Lond) 2006;56:307–311
18. Guzman KA, Taylor MR, Banfield JF. Environmental risks of nanotechnology: National Nanotechnology Initiative funding, 2000–2004. Environ Sci Technol 2006;40:1401–1407
19. Hardman R. A toxicologic review of quantum dots: toxicity depends on physicochemical and environmental factors. Environ Health Perspect 2006;114:165–172
20. Lanone S, Boczkowski J. Biomedical applications and potential health risks of nanomaterials: molecular mechanisms. Curr Mol Med 2006;6:651–663
21. Lawson CC, Grajewski B, Daston GP, Frazier LM, Lynch D, McDiarmid M, Murono E, Perreault SD, Robbins WA, Ryan MA, Shelby M, Whelan EA. Workgroup report: implementing a national occupational reproductive research agenda - decade one and beyond. Environ Health Perspect 2006;114:435–441
22. Moore MN. Do nanoparticles present ecotoxicological risks for the health of the aquatic environment? Environ Int 2006;32:967–976
23. Murr LE, Garza KM, Soto KF, Carrasco A, Powell TG, Ramirez DA, Guerrero PA, Lopez DA, Venzor J III. Cytotoxicity assessment of some carbon nanotubes and related carbon nanoparticle aggregates and the implications for anthropogenic carbon nanotube aggregates in the environment. Int J Environ Res Public Health 2005; 2:31–42
24. Nel A, Xia T, Madler L, Li N. Toxic potential of materials at the nanolevel. Science 2006;311:622–627
25. Oberdorster G, Oberdorster E, Oberdorster J. Nanotoxicology: an emerging discipline evolving from studies of ultrafine particles. Environ Health Perspect 2005;113:823–839
26. Robichaud CO, Tanzil D, Weilenmann U, Wiesner MR. Relative risk analysis of several manufactured nanomaterials: an insurance industry context. Environ Sci Technol 2005;39:8985–8994
27. Service RF. Nanotechnology: Calls rise for more research on toxicology of nanomaterials. Science 2005;310:1609
28. Wiesner MR. Responsible development of nanotechnologies for water and wastewater treatment. Water Sci Technol 2006;53:45–51
29. Worle-Knirsch JM, Pulskamp K, Krug HF. Oops, they did it again! Carbon nanotubes hoax scientists in viability assays. Nano Lett 2006;6:1261–1268
30. Adams LK, Lyon DY, Alvarez PJ. Comparative ecotoxicity of nanoscale TiO_2, SiO_2, and ZnO water suspensions. Water Res 2006; 40:3527–3532
31. Braydich-Stolle L, Hussain S, Schlager JJ, Hofmann MC. In vitro cytotoxicity of nanoparticles in mammalian germline stem cells. Toxicol Sci 2005;88:412–419
32. Fortner JD, Lyon DY, Sayes CM, Boyd AM, Falkner JC, Hotze EM, Alemany LB, Tao YJ, Guo W, Ausman KD, Colvin VL, Hughes JB. C_{60} in water: nanocrystal formation and microbial response. Environ Sci Technol 2005;39:4307–4316
33. Kim JS, Yoon TJ, Yu KN, Kim BG, Park SJ, Kim HW, Lee KH, Park SB, Lee JK, Cho MH. Toxicity and tissue distribution of magnetic nanoparticles in mice. Toxicol Sci 2006;89:338–347
34. Magrez A, Kasas S, Salicio V, Pasquier N, Seo JW, Celio M, Catsicas S, Schwaller B, Forro L. Cellular toxicity of carbon-based nanomaterials. Nano Lett 2006;6:1121–1125
35. Sayes CM, Gobin AM, Ausman KD, Mendez J, West JL, Colvin VL. Nano-C_{60} cytotoxicity is due to lipid peroxidation. Biomaterials 2005;26:7587–7595
36. Sayes CM, Wahi R, Kurian PA, Liu Y, West JL, Ausman KD, Warheit DB, Colvin VL. Correlating nanoscale titania structure with toxicity: a cytotoxicity and inflammatory response study with human dermal fibroblasts and human lung epithelial cells. Toxicol Sci 2006;92:174–185
37. Tian F, Cui D, Schwarz H, Estrada GG, Kobayashi H. Cytotoxicity of single-wall carbon nanotubes on human fibroblasts. Toxicol In Vitro 2006;20:1202–1212
38. Yamawaki H, Iwai N. Cytotoxicity of water-soluble fullerene in vascular endothelial cells. Am J Physiol Cell Physiol 2006;290: C1495–1502
39. Yang K, Zhu L, Xing B. Adsorption of polycyclic aromatic hydrocarbons by carbon nanomaterials. Environ Sci Technol 2006;40: 1855–1861
40. Zhu S, Oberdorster E, Haasch ML. Toxicity of an engineered nanoparticle (fullerene, C_{60}) in two aquatic species, *Daphnia* and the fathead minnow. Mar Environ Res 2006;62 Suppl:S5–9
41. Hoshino A, Fujioka K, Oku T, Suga M, Sasaki YF, Ohta T, Yasuhara M, Suzuki K, Yamamoto K. Physicochemical properties and cellular toxicity of nanocrystal quantum dots depend on their surface modification. Nano Lett 2004;4:2163–2169
42. Shiohara A, Hoshino A, Hanaki K, Suzuki K, Yamamoto K. On the cytotoxicity caused by quantum dots. Microbiol Immunol 2004;48: 669–675
43. Kako S, Santori C, Hoshino K, Gotzinger S, Yamamoto Y, Arakawa Y. A gallium nitride single-photon source operating at 200K. Nat Mater 2006;5:887–892
44. Ryman-Rasmussen JP, Riviere JE, Monteiro-Riviere NA. Surface coatings determine cytotoxicity and irritation potential of quantum dot nanoparticles in epidermal keratinocytes. J Invest Dermatol 2007;52:562–575
45. Zhang T, Stilwell JL, Gerion D, Ding L, Elboudwarej O, Cooke PA, Gray JW, Alivisatos AP, Chen FF. Cellular effect of high doses of silica-coated quantum dots profiled with high-throughput gene expression analysis and high-content cellomics measurements. Nano Lett 2006;6:800–808
46. Robichaud C, Tanzil D, Weilenmann U, Wiesner M. Relative risk analysis of several manufactured nanomaterials: an insurance industry context. Environ Sci Technol 2005;39:8985–8994
47. Lovric J, Bazzi HS, Cuie Y, Fortin GR, Winnik FM, Maysinger D. Differences in subcellular distribution and toxicity of green- and red-emitting CdTe quantum dots. J Mol Med 2005;83:377–385
48. Lovric J, Cho SJ, Winnik FM, Maysinger D. Unmodified cadmium telluride quantum dots induce reactive oxygen species formation leading to multiple organelle damage and cell death. Chem Biol 2005;12:1227–1234
49. Laffan R, Goldberg M, High J, Schaeffer T, Waugh M, Rubin B. Antihypertensive activity in rats for SQ 14225, an orally active inhibitor of angiotensin I-converting enzyme. J Parmacol Exp Ther 1978;204:281–288
50. Rubin B, Laffan R, Kotler D, O'Keefe E, Demaio D, Goldberg M. SQ 14225 (D-3 mercapto-2-methylpropanoyl-L-proline), a novel orally active inhibitor of angiotensin I-converting enzyme. Pharmacol Exp Ther 1978;204:271–280
51. Manabe N, Hoshino A, Liang Y, Goto T, Kato N, Yamamoto K. Quantum dot conjugated with medicine as a drug-tracer in vitro and in vivo. IEEE Trans NanoBiosci 2006;5:263–267
52. Pison U, Welte T, Giersig M, Groneberg DA. Nanomedicine for respiratory diseases. Eur J Pharmacol 2006;533:341–350
53. Bianco A, Kostarelos K, Prato M. Applications of carbon nanotubes in drug delivery. Curr Opin Chem Biol 2005;9:674–679
54. Lin H, Datar RH. Medical applications of nanotechnology. Natl Med J India 2006;19:27–32
55. Matsushita M, Tomizawa K, Moriwaki A, Li ST, Terada H, Matsui HJ. A high-efficiency protein transduction system demonstrating the role of PKA in long-lasting long-term potentiation. J Neurosci 2001;21:6000–6007
56. Haggie PM, Verkman AS. Diffusion of tricarboxylic acid cycle enzymes in the mitochondrial matrix in vivo. J Biol Chem 2002;277: 40782–40788
57. Dahan M, Levi S, Luccardini C, Rostaing P, Riveau B, Triller A. Diffusion dynamics of glycine receptors revealed by single quantum dot tracking. Science 2003;302:442–445
58. Goldman ER, Clapp AR, Anderson GP, Uyeda HT, Mauro JM, Medintz IL, Mattoussi H. Multiplexed toxin analysis using four colors of quantum dot fluororeagents. Anal Chem 2004;76:684–688
59. Gao X, Cui Y, Levenson RM, Chung LW, Nie S. In vivo cancer targeting and imaging with semiconductor quantum dots. Nat Biotechnol 2004;22:969–976
60. Voura EB, Jaiswal JK, Mattoussi H, Simon SM. Tracking metastatic tumor cell extravasation with quantum dot nanocrystals and fluorescence emission-scanning microscopy. Nat Med 2004;10:993–998
61. Arayne MS, Sultana N. Review: nanoparticles in drug delivery for the treatment of cancer. Pak J Pharm Sci 2006;19:258–268

62. Kim S, Lim YT, Soltesz EG, De Grand AM, Lee J, Nakayama A, Parker JA, Mihaljevic T, Laurence RG, Dor DM, Cohn LH, Bawendi MG, Frangioni JV. Near-infrared fluorescent type II quantum dots for sentinel lymph node mapping. Nat Biotechnol 2004;22:93–97
63. Parungo CP, Ohnishi S, Kim SW, Kim S, Laurence RG, Soltesz EG, Chen FY, Colson YL, Cohn LH, Bawendi MG, Frangioni JV. Intraoperative identification of esophageal sentinel lymph nodes with near-infrared fluorescence imaging. J Thorac Cardiovasc Surg 2005; 129:844–850
64. Samia AC, Chen X, Burda C. Semiconductor quantum dots for photodynamic therapy. J Am Chem Soc 2003;125:15736–15737
65. Warner JH, Hoshino A, Yamamoto K, Tilley RD. Water-soluble photoluminescent silicon quantum dots. Angew Chem Int Ed Engl 2005;44:4550–4554

NONLINEAR DYNAMICS OF INFECTIOUS DISEASES TRANSFER WITH POSSIBLE APPLICATIONS FOR TUBERCULAR INFECTION

V.D. Krevchik[1,5], T.V. Novikova[2], Yu. I. Dahnovsky[3], M.B. Semenov[1,5], E.V. Shcherbakova[1], Kenji Yamamoto[4]

[1] Physics Department, Penza State University, Penza 440017, Russia
physics@diamond.stup.ac.ru
[2] Penza regional tubercular prophylactic center, Russia
[3] Department of Physics & Astronomy/3905, 1000 E. University Ave., University of Wyoming, Laramie, WY, 82071, USA
[4] Research Institute of International Medical Center, Japan
backen@ri.imcj.go.jp
[5] Institute for Basic Research, P.O. Box 1577, Palm Harbor, FL 34682, USA
ibr@verizon.net

Received February 10, 2007

In this paper, we model a nonlinear dynamics of infectious diseases transfer. Particularly, we study possible applications to tubercular infection in models with different profiles (peak values) of the population density dependence on spatial coordinates. Our approach is based on the well known method of instantons which has been used by the authors to describe kinetics of adiabatic chemical reactions as a function of the heat-bath temperature and other system parameters. In our approach, we use "social temperature" T^* as one of the controlling parameters. Increase of T^* leads to acceleration of the infectious diseases transfer. The "blockage" effect for the infectious diseases transfer has been demonstrated in the case when peak values (in the population density) are equal to one and under condition that the "social temperature" is low. Existence of such effect essentially depends from environment "activity" (social and prophylactic). Results of our modeling qualitatively meet the tuberculosis dynamic spread data in Penza region of Russia.

Keywords: infectious diseases, transfer modeling.

1. Introduction

The problem of exact modeling of different types of infectious diseases transfer is of great importance [1, 2, 3, 4]. In most cases existing models are of "macroscopic" character (the scale is countrywide). A number of "macroscopic" models can be described as "network" models, percolation-, reactionary-diffusion-, oscillating, stochastic-, multivariable Markovian models [1], etc. Another type of models are of a microscopic character which are used at the molecular level: mutation models; models, which reveal infectious stability to different medicine influence, etc. Up to date, models of an intermediate (mesoscopic) level practically are not developed. Such models could give important (integrating) information about infectious "carrier" (like incubation period or latency). Also, such models would allow investigation of features of controllable infectious transfer at the scale of connecting settlements, e.g., towns.

Existing spectrum of the infectious transfer models has been discussed at the "International Symposium on Transmission Models for Infectious Diseases" [2, 3, 4] at the Tokyo International Medical Center of Japan, and vital necessity of the mesoscopic models for infectious transfer has been convincingly demonstrated. Although the most reports at this Conference has been devoted to modeling of the supposed global pandemic influenza (with account for high risks and for the infectious transfer high rates); the mesoscopic model for the tuberculosis transfer has been recognized as important one as well. Importance of the research at this level can be also confirmed by the integrated statistics for the tuberculosis diseases growth in Russia since 1991 (see Fig. 1). This tendency is kept today in Russia, and problem is complicated because of high population decrease (see Fig. 2).

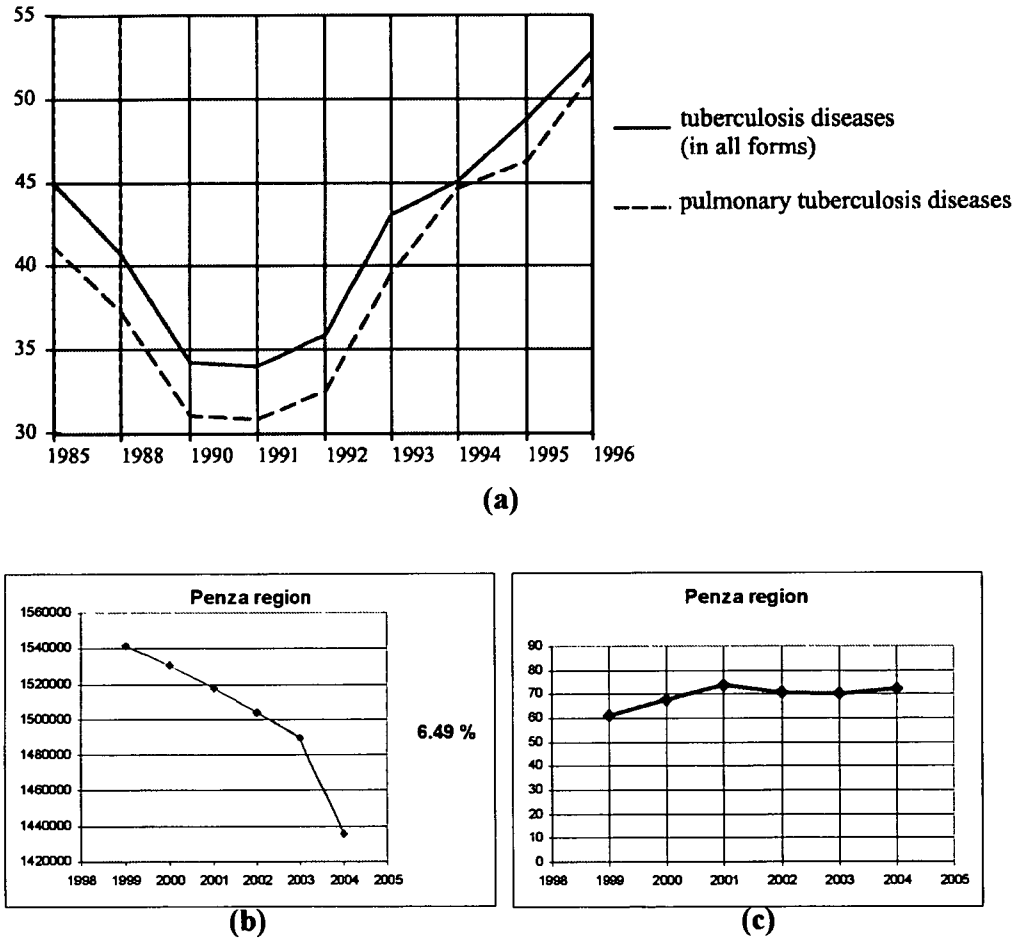

Fig. 1. (a) Tendencies for the tuberculosis diseases growth in Russia since 1991; (b) Population decrease in Penza region, Russia; (c) Tuberculosis diseases growth in Penza region, Russia.

2. The model description

Prior to mathematical formulation of the model, we will discuss on some assumptions. For example, with an account for the tuberculosis diseases features

(as social diseases), preferential (or probable) directions of infectious transfer are directions from settlements (towns) with lower population density (Fig. 3) to settlements with higher population density. The infection transfer rate essentially depends from social-economic conditions, which we indirectly describe by the "social temperature" parameter. With higher "social temperature", more complicated social-economic conditions are realized (unemployment level increases, inflation increases, medical service for the essential population part is getting worse, etc.); as the result, infectious transfer rate becomes higher. Environment (where infection transfers) essentially influence on the infectious disease transfer dynamics. Particularly, active prophylactics can increase resistibility (or "dissipation") of environment to the infectious disease transfer. On the other hand, destabilizing or excitation (oscillating) influence on the environment can lead to the infectious transfer rate growth. Besides, "inertia", which is related to incubation period of disease, can be included in the model through the parameter similar to "mass". All the abovementioned factors are considered in suggested mesoscopic model.

To construct the model, we develop and apply well approved instanton method, which has been used earlier in dissipative tunnel chemical kinetics research (with account of the heat bath influence) [5, 6]. For this purpose, we will specify the formulation of transfer (kinetic) problem and will show how Hamiltonian of the initial reactionary system can be transformed to the traditional one, which can describe transfer with account of "dissipation". To make it, we introduce the reaction coordinate (infectious transfer direction); and the potential profile along this coordinate will be of the form shown in Fig. 2.

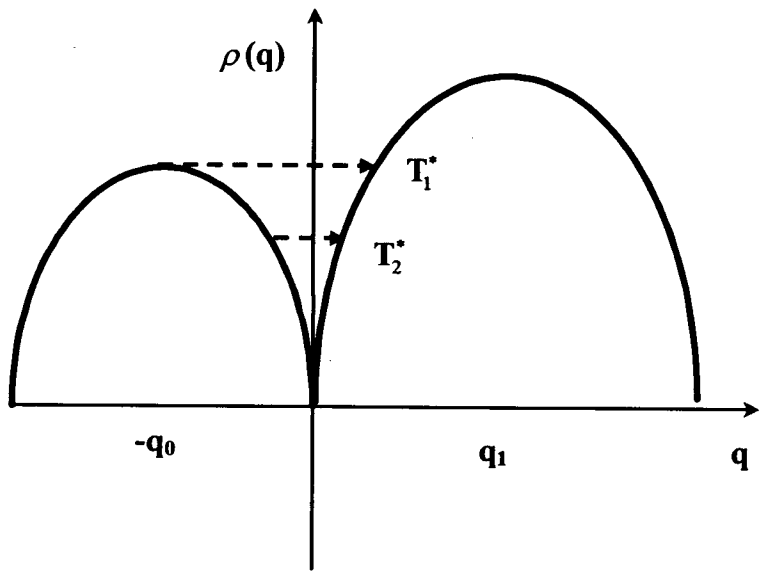

Fig. 2. Distribution of an infection (of infectious diseases transfer) along a line connecting two neighbor settlements with various population density $\rho(q)$, depending on "social temperature" T^* ($T_2^* > T_1^*$).

The condition of the reacting system in an environment is determined by the multidimensional potential energy surface. Appropriate approximation to study "low temperature" kinetics at such a surface is the following potential energies:

$$U_i = \sum_{i=1}^{N} \frac{1}{2} \omega_{0i}{}^2 (x_i + x_{0i})^2, \quad U_f = \sum_{i=1}^{N} \frac{1}{2} \omega_{0i}{}^2 (x_i - x_{0i})^2 - \Delta \mathrm{I}. \qquad (1)$$

At low temperatures the potential energy terms of the initial and final states are assumed to be presented as the set of oscillators with frequencies ω_{0i}, relatively shifted to $2x_{oi}$, the oscillator "masses" are chosen to be equal to 1 , hence, their coordinates are renormalized to the square root of the cor-

responding mass. The term of the final state lies lower than the initial one by the value of ΔI (the "reaction heat" or asymmetry parameter in the population density profile).

The plane, being the intersection surface of the two paraboloids, is determined by the equation:

$$2\lambda\sum_{i=1}^{N}\gamma_i x_i = -\Delta \mathrm{I}, \tag{2}$$

where

$$\gamma_i = \frac{1}{\lambda} x_{0i}\omega_{0i}{}^2, \tag{3}$$

$$\lambda^2 = \sum_{i-1}^{N}\omega_{0i}{}^4 x_{0i}{}^2 \tag{4}$$

so that the normalization condition is fulfilled,

$$\sum_{i=1}^{N}\gamma_i{}^2 = 1. \tag{5}$$

The coordinate normal to the plane (2) stands for a transfer coordinate. Let us select it out of the whole coordinate set so that the remaining in the plane (2) $(N-1)$ oscillators are mutually independent but and only linearly connected with the chosen transfer coordinate. For this aim we consider the orthogonal rotation of the coordinate system, so that one coordinate coincides with the transfer one:

$$y_1 = \sum_{i=1}^{N}\gamma_i x_i, \tag{6}$$

whereas the other $(N-1)$ coordinates diagonalize the potential energy in the plane (2):

$$y_j = \sum_{i-1}^{N} U_{ji} x_i , \tag{7}$$

and $U_{1i} = \gamma_i$. The quadratic form $\sum_{i=1}^{N} \omega_{0i}{}^2 x_i{}^2$ may be transformed to

$$\omega_1{}^2 y_1{}^2 + 2 y_1 \sum_{\alpha=2}^{N} C_\alpha y_\alpha + \sum_{\alpha=2}^{N} \omega_\alpha{}^2 y_\alpha{}^2 , \tag{8}$$

where $\omega_\alpha{}^2$ satisfies the equation for eigenvalues. To obtain this equation we should diagonalize the quadratic form

$$\sum_{i-1}^{N} \omega_{0i}{}^2 x_i{}^2 , \tag{9}$$

Under condition that the transfer coordinate is determined by Eq. (6), and other oscillators coordinates are chosen so that there are not terms of $y_i y_\alpha$ - type $(i, \alpha \geq 2)$, but there are terms of the transfer coordinate y_1 interaction with coordinates y_i $(i \geq 2)$. For this purpose we should fulfill diagonalization of the quadratic form:

$$\sum_{i=1}^{N} \omega_{0i}{}^2 U_{\alpha i} U_{\alpha' i} = \omega_i{}^2 \delta_{\alpha\alpha'} , \tag{10}$$

where $U_{\alpha i}$ is element of an orthogonal matrix. Let's multiply both parts of this equation on $U_{\alpha' i}$ and make summation over α' from 2 to N with an account for the orthogonality condition for the matrix of transformation,

$$U_{\alpha k} = \frac{\gamma_k C_\alpha}{\omega_{0k}^{\ 2} - \omega_\alpha^{\ 2}}, \tag{11}$$

where

$$C_\alpha = \sum_{i=1}^{N} \omega_{0i}^{\ 2} \gamma_i U_{\alpha i}. \tag{12}$$

Substituting $U_{\alpha k}$ from (11) to (12), we obtain the equation, which determines the eigenvalues $\omega_\alpha^{\ 2}$,:

$$\sum_{i=1}^{N} \frac{\omega_{0i}^{\ 2} \gamma_i^{\ 2}}{\omega_{0i}^{\ 2} - \omega_\alpha^{\ 2}} = 1. \tag{13}$$

One eigenvalue $\omega_1^{\ 2} = 0$ should be excluded from the consideration. With an account for Eq. (5), the equation (13) can be transformed to following form:

$$\sum_{i=1}^{N} \frac{\gamma_i^{\ 2}}{\omega_{0i}^{\ 2} - \omega_\alpha^{\ 2}} = 0. \tag{14}$$

Let's define now factors C_α from Eq. (12) and orthogonality conditions for the matrix of transformation:

$$C_\alpha = \left[\sum_{i=1}^{N} \frac{\gamma_i^{\ 2}}{\left(\omega_{0i}^{\ 2} - \omega_\alpha^{\ 2}\right)^2} \right]^{-1/2}. \tag{15}$$

Let's note, that

$$\omega_1^{\ 2} = \sum_{i=1}^{N} \omega_{0i}^{\ 2} \gamma_i^{\ 2}, \tag{16}$$

Hence, the system Hamiltonian may be written as:

$$\hat{H} = \frac{p_1^{\ 2}}{2} + v_1(y_1) + y_1 \sum_{\alpha=2}^{N} C_\alpha y_\alpha + \frac{1}{2} \sum_{\alpha=2}^{N} \left(p_\alpha^{\ 2} + \omega_\alpha^{\ 2} y_\alpha^{\ 2} \right), \tag{17}$$